ASIAN JOURNAL OF PHARMACEUTICAL AND CLINICAL RESEARCH

INNOVARE ACADEMIC SCIENCES
Knowledge to Innovation

Vol 18, Issue 8, 2025

Online - 2455-3891
Print - 0974-2441

Research Article

IDENTIFICATION OF POTENTIAL INHIBITORS OF A-GLUCOSIDASE ENZYME FROM *WITHANIA COAGULANS* AND *SWIETENIA MACROPHYLLA* USING GC-MS PROFILING, *IN SILICO* MOLECULAR DOCKING AND MOLECULAR DYNAMICS SIMULATION STUDIES

ROSLIN ELSA VARUGHESE, GAYATHRI DASARARAJU*

Centre of Advanced Study in Crystallography and Biophysics, University of Madras, Chennai, Tamil Nadu, India.
***Corresponding author: Gayathri Dasararaju; Email: drdgayathri@gmail.com**

Received: 8 May 2025, Revised and Accepted: 20 June 2025

ABSTRACT

Objective: Diabetes mellitus, a global health concern, is characterized by persistently elevated blood glucose levels, which can lead to damage in various organs over time. The enzyme α-glucosidase plays a critical role in carbohydrate digestion by hydrolyzing complex polysaccharides into absorbable monosaccharides. Inhibition of this enzyme helps attenuate postprandial hyperglycemia by delaying carbohydrate breakdown and absorption. In the present study, we aimed to identify potential natural α-glucosidase inhibitors from the ethyl acetate and ethanol extracts of two medicinally essential plants: *Withania coagulans* and *Swietenia macrophylla*.

Methods: Gas chromatography–mass spectrometry analysis was carried out to identify the compounds, which were subjected to virtual screening against α-glucosidase using AutoDock Vina. The top three ligands from each extract were further validated through re-docking using AutoDock 4.2, allowing for detailed analysis of binding energies and interactions within the enzyme's active site. The top lead compounds from docking results were subjected to molecular dynamics (MD) simulation studies.

Results: Cholest-5-ene-3,16,22,26-tetrol (from *W. coagulans*) and 1,5-Anhydro-4,6-O-benzylidene-D-glucitol (from *S. macrophylla*) exhibited better binding energies of –6.66 and –5.64 kcal/mol, respectively, compared to the reference inhibitor acarbose (–4.27 kcal/mol). These lead complexes were further subjected to MD simulations to assess the conformational stability and structural dynamics of the enzyme-compound complexes. The average root-mean-square deviation for the last 50 ns of enzyme-lead complexes was found to be 0.14 and 0.16 nm.

Conclusion: The identified compounds show good binding energy and maintain the hydrogen bond and hydrophobic interactions with active site residues of the enzyme. This study highlights the potential of plant-derived phytochemicals as promising α-glucosidase inhibitors and provides a computational foundation for their further *in vitro* and *in vivo* evaluation in the management of diabetes mellitus.

Keywords: *Withania coagulans*, *Swietenia macrophylla*, AutoDock Vina, Screening, Molecular docking, Molecular dynamics simulation

 DOI: http://dx.doi.org/10.22159/ajpcr.2025v18i8.55102. Journal homepage: https://innovareacademics.in/journals/index.php/ajpcr

INTRODUCTION

Diabetes mellitus (DM) is a long-term metabolic condition marked by consistently high blood glucose levels due to inadequate insulin production, resistance to insulin action, or a combination of both factors. It is a global health concern, with rising prevalence associated with sedentary lifestyles, dietary habits, and genetic vulnerability. Persistent high blood sugar levels in diabetes can cause progressive damage and impaired function in multiple organs, especially the eyes, kidneys, nerves, heart, and blood vessels. Accounting for approximately 90–95% of all diabetes cases globally, type 2 diabetes mellitus (T2DM) has become a significant public health concern due to its rising prevalence, particularly in low- and middle-income countries.

One of the therapeutic strategies for managing postprandial hyperglycemia in T2DM involves inhibiting enzymes responsible for carbohydrate digestion, particularly α-glucosidase. α-Glucosidase is an essential enzyme found in the brush border of the small intestine, responsible for breaking down terminal, non-reducing 1,4-linked α-glucose units. This reaction plays a crucial role in the final phase of carbohydrate digestion and the subsequent absorption of glucose. Inhibiting this enzyme delays glucose release from complex carbohydrates, thereby attenuating postprandial blood glucose spikes. Clinically used α-glucosidase inhibitors such as acarbose, voglibose, and miglitol have demonstrated efficacy in glycemic control; however, their use is often limited by gastrointestinal side effects [1].

Consequently, there is growing interest in identifying novel, naturally derived α-glucosidase inhibitors with improved efficacy and safety profiles. Phytochemicals from medicinal plants have emerged as promising candidates due to their structural diversity and multifunctional properties, offering potential for the development of effective antidiabetic therapies. Therefore, in this study, we have used two medicinally useful plants as the source to identify the important phytochemicals against α-glucosidase enzyme.

Withania coagulans, commonly referred to as "Paneer Dodi" or "Indian cheese maker," is a medicinal shrub belonging to the *Solanaceae* family. It is mainly found in different parts of India, Pakistan, and Afghanistan. Conventionally, various parts of the plant have been utilized to manage ailments such as diabetes [2,3], inflammation [4], liver disorders [5], and microbial infections [6,7]. This plant is rich in withanolides, a group of steroidal lactones, including Coagulin F and Coagulin G. Withaferin A and Withanolide E have been reported to exhibit immunosuppressive activity by modulating the function of human B and T lymphocytes, as well as mouse thymocytes [8]. Other phytochemical constituents of the plant consist of alkaloids, flavonoids, saponins, tannins, phenolic compounds, carbohydrates, and organic acids. Methanolic extracts of the fruit of the plant have demonstrated significant enhancement in glucose uptake in yeast cells, indicating antihyperglycemic properties [9]. Furthermore, aqueous extracts have shown inhibitory effects on the α-glucosidase enzyme, which is pivotal in carbohydrate digestion, thereby aiding in postprandial blood glucose regulation.

Studies have reported that methanolic and aqueous extracts of the plant can suppress the production of pro-inflammatory mediators. This can be attributed to the presence of withanolides, which modulate inflammatory pathways, including the inhibition of nuclear factor kappa B activation and the upregulation of Nrf2-mediated antioxidant responses [10,11]. These include antimicrobial, hepatoprotective, immunomodulatory, and anticancer effects.

Swietenia macrophylla, widely referred to as big-leaf mahogany, is a deciduous tree species that belongs to the *Meliaceae* family. Native to Central and South America, it is widely cultivated in tropical and subtropical regions for its high-quality timber. Beyond its economic value, *S. macrophylla* has gained attention in traditional and modern medicine due to its diverse pharmacological properties. Different parts of *S. macrophylla* have been traditionally used in folk medicine across various Asian countries to manage a wide range of health conditions. Numerous phytochemical and pharmacological studies have substantiated the medicinal value of the plant's extracts. Leaf extracts prepared using methanol, dichloromethane, and n-hexane have shown significant antibacterial and antioxidant activities [12]. The methanolic seed extract has been experimentally shown to exert hypoglycemic and hypolipidemic effects [13]. Various extracts of the plant are shown to have antiviral, antidiabetic, antitumor, anticancer, antimutagenic, and anti-inflammatory effects [14]. The aqueous extract of the leaves of the plant was shown to have a cytoprotective effect [15].

The therapeutic potential of *W. coagulans* and *S. macrophylla* continues to be explored through both *in vitro*, *in vivo*, and *in silico* studies, making it a promising candidate for natural product-based drug discovery. In the present study, we have used the ethyl acetate and ethanol extracts of the plants to identify compounds using gas chromatography–mass spectrometry (GC-MS) analysis and investigate its inhibitory potential against α-glucosidase enzyme. We have also utilized *in silico* approaches, including molecular docking and molecular dynamics (MD) simulations, to investigate the interaction of selected compounds with α-glucosidase enzyme.

METHODS

Extraction

The dried fruits of *W. coagulans* and seeds of *S. macrophylla* were purchased in large quantities from a local Ayurvedic shop in Chennai, Tamil Nadu. 50 g of *W. coagulans* fruits were crushed in an oil extractor. Similarly, 50 g of *S. macrophylla* seeds obtained after removing the husks were subjected to a gentle blending process. Sequential solvent extraction was carried out for each sample. Initially, 200 mL of petroleum ether was added to the plant material and macerated for 72 h at room temperature. The resulting extract underwent filtration using Whatman filter paper to remove particulate matter. Subsequently, the filtrate was concentrated by employing a rotary evaporator under reduced pressure and controlled temperature, facilitating efficient removal of excess solvent. The plant sample was then air-dried and subjected to subsequent extractions using 200 mL of dichloromethane, ethyl acetate, and ethanol, each macerated for 72 h. Each solvent-derived extract was individually processed by filtering and followed by concentrating using a rotary evaporator (LabTech company).

The ethyl acetate and ethanol extracts of *W. coagulans* yielded 1.2 g and 1.1 g of concentrated sample, respectively. For *S. macrophylla*, the respective yields were 1.0 g (ethyl acetate) and 1.3 g (ethanol). The concentrated extracts were transferred into airtight containers and stored at 4 °C to ensure sample stability and reduce the risk of degradation until further analysis.

GC-MS analysis

Phytochemical profiling for the four extracts was performed using a Shimadzu GCMS-QP2010 Plus system equipped with an electron ionization source and an autosampler. 1 µL of each sample was injected into the GC-MS system. The GC oven was initially maintained at a temperature of 50°C for 1 min and then ramped to 280°C at the rate of 10°C/min for a period of 2 min. Helium served as the carrier gas, maintained at a steady flow rate of 1 mL/min to ensure consistent chromatographic performance. The sample was introduced through an injection port set at 250°C, utilizing a split ratio of 50:1 to regulate the sample volume entering the column. To facilitate effective ionization of analytes, the interface temperature was held at 280°C, while the ion source operated at 200°C. The mass-spectrometer facilitated the scan across a mass-to-charge (m/z) range of 40–700, allowing the detection of all ions within that range, providing a complete mass spectrum of the compounds eluted. The spectral data were then compared with the National Institute of Standards and Technology mass spectral library for identifying the detected compounds.

Molecular docking

Molecular docking is a pivotal computational technique widely employed in drug discovery to evaluate interactions between proteins and biologically active small molecules. In this study, the N-terminal catalytic domain of human intestinal maltase-glucoamylase (NtMGAM), represented by PDB ID: 2QMJ [16], was chosen as the receptor, which was retrieved from the Protein Data Bank [17]. The protein molecule was prepared by assigning Kollman charges, removing crystallographic water molecules, and adding polar hydrogens.

The 3D structure of the receptor molecule was retrieved from the Protein Data Bank. The phytochemicals identified from GC-MS analysis were subjected to molecular docking studies. The three-dimensional coordinates of these compounds were either downloaded in SDF format from the PubChem database [18] or drawn manually using ChemDraw [19] in MOL format. The SDF or MOL format files were converted to PDB using a custom Open Babel [20] automation script. During the conversion, three-dimensional coordinates were generated, and energy minimization was performed using the Universal Force Field with a maximum of 50,000 steps to obtain the lowest-energy conformers. The resulting PDB files were further converted to PDBQT format, which included assignment of torsions and addition of Gasteiger charges, using Open Babel as well.

Virtual screening: AutoDock Vina

An automated shell script was employed to perform batch screening of GC-MS-identified compounds using AutoDock Vina 1.1.2 [21]. All ligands processed in PDBQT format were placed in a directory. A custom configuration file (config.txt) was created, specifying the grid box center and dimensions around the active site of the receptor protein. The search space for docking was defined using the following parameters: center_x = −19.378, center_y = −5.879, center_z = −11.938; size_x = 20, size_y = 20, size_z = 20 (in Å), based on the known active site coordinates of the protein structure (PDB ID: 2QMJ). Vina was executed with default exhaustiveness, and all ten conformations for each ligand, ranked by their binding affinities, were generated as the output.

A custom script was employed for post-processing and sorting of AutoDock Vina results. It was used to extract the lowest binding energy of the top ten ligands. The ligands were arranged in order of increasing binding energy, with those exhibiting the most negative values (indicative of stronger binding affinities) placed at the top of the list. Top 10 ligands were automatically copied into a separate folder for further structural and energetic analysis. This workflow enabled the identification of high-affinity compounds for further validation.

Validation using AutoDock 4.2

Validation for the best-docked ligands was performed using AutoDock 4.2 [22], which applies the Lamarckian Genetic Algorithm to explore ligand conformational space within the receptor's binding site. Before docking, both ligand and protein structures were prepared by the method as mentioned earlier.

The NtMGAM enzyme (~100 kDa) consists of 868 amino acids distributed across five structural domains: a trefoil type-P domain, a β-sandwich domain at the N-terminus, a catalytic $(\beta/\alpha)_8$ barrel

domain with insertions, and two C-terminal domains. The active site, located in the $(\beta/\alpha)_8$ barrel domain, plays a critical role in hydrolyzing carbohydrates by cleaving glycosidic bonds. A grid box with dimensions 60 × 54 × 58 Å and grid spacing of 0.375 Å was centered over the active site to encompass key catalytic residues: Asp203, Tyr299, Asp327, Ile328, Ile364, Trp406, Trp441, Asp443, Met444, Arg526, Trp539, Asp542, Phe575, Ala576, and His600 [16]. AutoDockTools was used to analyze the ten docking poses generated, and binding interactions were further visualized using LigPlot+ [23], focusing on ligand binding energy and contacts with active site residues.

MD simulation

MD simulations were conducted using GROMACS2018.1 [24] to evaluate the dynamic behavior of the compounds when bound to the active site of the enzyme. For comparison of the results, the enzyme-acarbose complex was also subjected to MD simulation after docking studies. Each protein–ligand complex was simulated for a total duration of 100 ns to assess structural stability and binding consistency. The CHARMM27 [25] force field was used for all simulations, and the systems were solvated in a cubic box filled with SPC (Simple Point Charge) water molecules. Topology files for the ligands were prepared using the SwissParam [26,27] server, and each system was neutralized by the addition of 29 Na^+ ions.

Energy minimization was executed using the steepest descent algorithm, concluding when the maximum force reaches a threshold of 1000 kJ/mol/nm. The minimized systems were then subjected to a two-step equilibration process: Beginning with a 100 ps simulation under the NVT ensemble (constant Number of particles, Volume, and Temperature) to stabilize temperature at 300 K using the velocity-rescaling thermostat. This was followed by a 100 ps NPT ensemble (constant Number of particles, Pressure, and Temperature) simulation, where pressure was regulated at 1 bar employing the Berendsen barostat. These steps ensured the system achieved thermal and pressure equilibrium, providing a stable foundation for further MD simulations.

During the production MD simulation, the system's temperature was regulated using the Nosé–Hoover thermostat, while pressure control was achieved through the Parrinello–Rahman barostat, ensuring accurate sampling of the isothermal-isobaric (NPT) ensemble, maintaining thermal and pressure stability throughout the simulation. Structural and dynamic analyses were carried out using built-in GROMACS tools, including evaluation of root-mean-square deviation (RMSD), root-mean-square fluctuation (RMSF), radius of gyration (Rg), hydrogen bonding, and solvent-accessible surface area (SASA). The resulting data were visualized using Xmgrace [28] software.

RESULTS AND DISCUSSION

GC-MS compound identification

This study provides a promising approach to develop plant compounds for diabetic control and treatment. Antidiabetic activity of novel chromene compounds from *Peperomia pellucida* L. Kunth [29] and compounds from *Laserpitium latifolium* L [30] were reported and several plant compounds were also reported and are being examined for their potential in diabetic control. The identification of volatile components from *W. coagulans* and *S. macrophylla* was performed using GC-MS analysis. Lists of few compounds that were identified from each extract are tabulated in Tables 1-4 along with their area percentage, retention time, and molecular weight.

Molecular docking

Screening of compounds using AutoDock Vina

A comprehensive virtual screening workflow was carried out using AutoDock Vina to evaluate the binding potential of phytochemical compounds identified from the ethyl acetate (EA) and ethanol (EtOH)

Table 1: Few identified compounds from the ethyl acetate extract of *Withania coagulans*

Compound name	Area%	Retention time	Molecular weight (g/mol)
4-(3-hydroxypropyl)-2-methoxyphenol	0.52	16.325	182.22
1-*O*-butyl 2-*O*-(5-methylhexan-2-yl) benzene-1,2-dicarboxylate	1.51	19.975	320.40
Hexadecanoic acid	5.56	19.605	256.42
Dibutyl benzene-1,2-dicarboxylate	2.50	19.765	278.34
Octadeca-9,12-dienoic acid	16.77	21.395	280.40
(*Z*)-Tricos-9-ene	2.10	21.865	322.60
Dodecyl 2-fluoroacetate	0.63	22.020	246.36
2-(3-methylpent-1-yn-3-yloxycarbonyl) benzoic acid	0.47	22.340	246.26
2-[5-methyl-3-(trifluoromethyl)-1H-pyrazol-1-yl] acetamide	0.18	22.470	207.15
2-(Ethylenedioxy) ethylamine, N-methyl-N-[4-(1-pyrrolidinyl)-2-butynyl]	0.13	23.815	252.35
E, E, Z-1,3,12-Nonadecatriene-5,14-diol	0.47	24.009	294.50
2H-Pyran-3-ol, tetrahydro-2,2,6-trimethyl-6-(4-methyl-3-cyclohexen-1-yl)-, [3S-[3.alpha.,6.alpha.(R*)]]-	0.35	24.990	238.37
Bis (2-ethylhexyl) benzene-1,2-dicarboxylate	6.85	25.180	390.60

Table 2: List of compounds identified from the ethanol extract of *Withania coagulans* fruits

Compound name	Area %	Retention time	Molecular weight (g/mol)
Methyl 2,3-di-O-acetyl-4-O-methyl-.alpha.-D-xylopyranoside	1.19	13.025	262.26
4-((1E)-3-Hydroxy-1-propenyl)-2-methoxyphenol	1.24	17.420	180.20
Hexadecanoic acid	1.20	19.605	256.42
Octadeca-9,12-dienoic acid	1.83	21.385	280.40
2,8-diethoxy-1,7-diazatricyclo[7.3.0.0^{3,7}]dodeca-2,8-diene	0.48	22.945	250.34
Ergotaman-3',6',18-trione, 9,10-dihydro-12'-hydroxy-2'-methyl-5'-(phenylmethyl)-, (5'.alpha.,10.alpha)	0.20	23.620	583.70
1,4,7-Androstatrien-3,17-dione	1.29	24.610	282.40
Androst-4-en-9-thiocyanomethyl-11-ol-3,17-dione	0.79	24.840	373.50
Dioctyl benzene-1,2-dicarboxylate	0.73	25.190	390.60
Andrographolide	0.17	25.450	350.40
Cholest-5-ene-3,16,22,26-tetrol	0.50	25.755	434.70

Table 3: List of compounds identified from the ethyl acetate extract for the seeds of *Swietenia macrophylla*

Compound name	Area%	Retention time	Molecular weight (g/mol)
3-phenyl-*N*-(1,3-thiazol-2-yl) propanamide	0.02	14.280	230.29
(1,7,7-trimethyl-2-bicyclo[2.2.1]heptanyl) 3-propan-2-ylidenecyclopentane-1-carboxylate	0.07	16.695	290.40
4-Carbamoyl-2-phenyl-2-oxazoline	0.10	20.771	190.20
(3*E*,12*Z*)-Nonadeca-1,3,12-triene-5,14-diol	28.63	21.470	294.50
Octadecanoic acid	11.54	21.645	284.50
(*E*)-2-methyl-4-(1,3,3-trimethyl-7-oxabicyclo[4.1.0]heptan-2-yl) but-3-en-2-ol	1.70	22.155	224.34
(6*S*)-3-methyl-6-[(2*S*)-6-methyl-4-oxohept-5-en-2-yl] cyclohex-2-en-1-one	0.48	22.340	234.33
Glycidyl palmitate	0.76	22.875	312.50
(14*R*)-14-methylhexadec-8-yn-1-ol	1.49	24.445	252.40
1,3-dihydroxypropan-2-yl hexadecanoate	1.03	24.785	330.50
1-acetyl-2-depentyl-Perhydro-htx-8-one	0.10	25.265	265.39

Table 4: List of few compounds identified from the ethanol extract of *Swietenia macrophylla* seeds

Compound name	Area%	Retention time	Molecular weight (g/mol)
Ethyl hexadecanoate	0.96	13.195	284.50
(*Z*)-Hexadec-9-enal	17.45	14.215	238.41
Ergotaman-3',6',18-trione, 9,10-dihydro-12'-hydroxy-2'-methyl-5'-(phenylmethyl)-, (5'.alpha.,10.alpha.)-	0.17	15.985	583.70
Propan-2-yl 6-(4-fluorophenyl)-3-methyl-4-oxo-1,5,6,7-tetrahydroindole-2-carboxylate	0.11	17.500	329.40
Phenyl-(5-phenylthiazol-2-yl)-amine	0.06	19.975	252.30
Bis (2-propan-2-yloxyphenyl) pentanedioate	0.10	20.270	400.50
1,5-Anhydro-4,6-O-benzylidene-D-glucitol	0.40	20.730	252.26
9-Cycloheptatrienylidene-9,10-dihydro-10-oxoanthracene	0.02	20.921	282.30
Abietic acid	0.48	21.970	302.50
17-epi-Pregnenolone	0.17	24.000	316.50
Pregna-5,14-diene-3,20-diol-18-carboxylic acid, 3-acetate-, lactone	0.68	24.980	370.50
Cycloeucalenyl acetate	0.29	26.785	468.80

extracts of two plant species, *W. coagulans* and *S. macrophylla*. These extracts were profiled through GC-MS analysis, and the resulting compounds were subjected to docking after the initial preparation of the ligand molecules. During molecular docking of the ligand molecules with the target enzyme, water molecules were excluded from the enzyme.

In total, 371 unique ligands were screened against the target enzyme α-glucosidase (PDB ID: 2QMJ), where 83 ligands from the EA extract of *W. coagulans*, 86 ligands from the EtOH extract of *W. coagulans*, 90 ligands from the EA extract of *S. macrophylla*, and 112 ligands from the EtOH extract of *S. macrophylla*.

The screening aimed to identify potential α-glucosidase inhibitors by ranking the compounds based on their binding energy values, with more negative values indicating stronger predicted affinities. The top ligands from each extract exhibited good interaction with the active site of α-glucosidase enzyme, mainly through hydrophobic and hydrogen bond interactions.

Validation using AutoDock 4.2

To further validate the binding interactions, three ligands were selected from the top hits of AutoDock Vina based on their binding energy and were subsequently re-docked using AutoDock 4.2. Based on available literature, acarbose is known to form hydrogen bonds with key residues of the NtMGAM active site, including Asp203, Asp327, Arg526, Asp542, His600, and Tyr605. In the control docking study in AutoDock 4.2, acarbose was observed to form hydrogen bonds with residues Asp203, Tyr299, Asp327, Arg334, and Asp542. The binding energy for the enzyme-acarbose complex was −4.27 kcal/mol. The binding energy values for the three docked compounds identified from *W. coagulans* and *S. macrophylla* for both the extracts are summarized in Table 5 and Table 6, respectively. The two compounds showing better interactions and binding energies, Cholest-5-ene-3,16,22,26-tetrol (compound 1) and 1,5-Anhydro-4,6-O-benzylidene-D-glucitol (compound 2), derived from *W. coagulans* and *S. macrophylla*, exhibited binding energies of −6.66 and −5.64 kcal/mol, respectively. These ligands demonstrated favourable interactions within the active site, forming multiple hydrogen bonds and hydrophobic contacts with catalytic residues, as visualized using LigPlot+ (Figs. 1 and 2). These ligands showed strong binding within the α-glucosidase active site, particularly interacting through hydrogen bonds with key residues such as Asp203, Phe450, Arg526, Asp542, and Gln603 for compound1 and Asp203 and Asp542 for compound 2 (Table 7).

MD simulation

To investigate the conformational stability and flexibility of the ligand-bound α-glucosidase complexes, MD simulations were carried out for a duration of 100 ns. The trajectories of the enzyme–ligand complexes were compared with that of the enzyme bound to its co-crystallized ligand, acarbose. Two lead compounds, compound 1 and compound 2, were chosen for simulation based on their strong binding affinities and hydrogen bond interactions observed from the molecular docking study. The simulations were performed using GROMACS, and key structural metrics such as, RMSD, RMSF, Rg, number of hydrogen bonds, and SASA, were assessed. These analyses provided insights into the dynamic stability and interaction profiles of compound 1, compound 2, and acarbose within the active site of α-glucosidase.

The RMSD graph is widely used to evaluate the structural stability of a biomolecular system upon ligand binding and whether the complex reaches a conformational equilibrium over time. The RMSD for the protein backbone atoms for acarbose showed a significant increase after 40 ns and gradually attains equilibrium by the end of 100 ns simulation. Compound 1 in complex with the enzyme shows an initial increase but then decreases and maintains a stable trajectory till 100 ns. For the compound 2-enzyme complex, after an initial increase, the complex attains stability till the end of the simulation. The average RMSD for the last 50 ns of the enzyme-acarbose complex was found to be 0.15 nm, while it was 0.14 and 0.16 nm for enzyme-compound 1 and

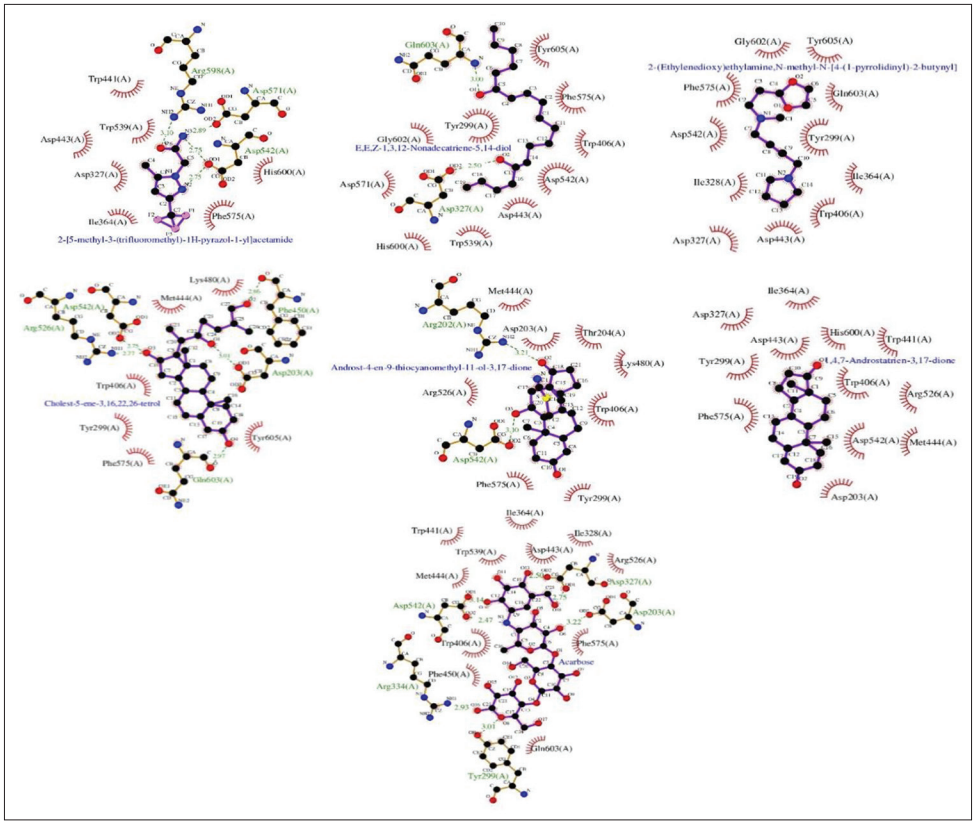

Fig. 1: Ligand interactions for the re-docked compounds identified from ethyl acetate and ethanol extracts of *Withania coagulans*. Interactions of acarbose with the enzyme is also shown

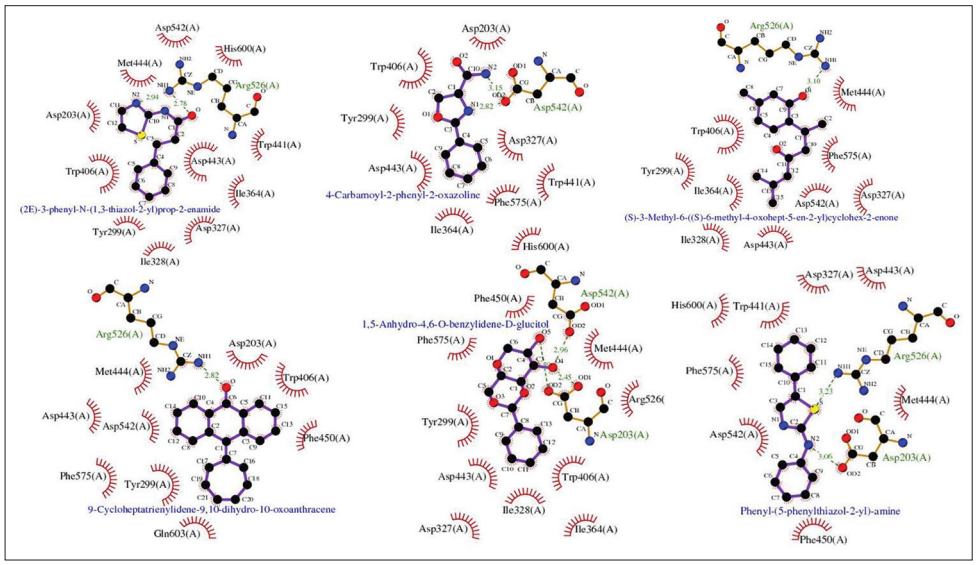

Fig. 2: Ligand interactions for re-docked compounds screened from the ethyl acetate and ethanol extracts of *Swietenia macrophylla*

Table 5: Binding energies for the top three ligands re-docked after the screening from ethyl acetate and ethanol extracts of *Withania coagulans*

Compound name (Ethyl acetate extract)	Binding energy (kcal/mol)	Compound name (Ethanol extract)	Binding energy (kcal/mol)
2-[5-methyl-3-(trifluoromethyl)-1H-pyrazol-1-yl] acetamide	−5.17	1,4,7-Androstatrien-3,17-dione	−6.56
E, E, Z-1,3,12-Nonadecatriene-5,14-diol	−4.72	Cholest-5-ene-3,16,22,26-tetrol	−6.66
2-(Ethylenedioxy) ethylamine, N-methyl-N-[4-(1-pyrrolidinyl)-2-butynyl]	−8.84	Androst-4-en-9-thiocyanomethyl-11-ol-3,17-dione	−6.57

enzyme-compound 2, respectively. This shows that the enzyme is stable when in complex with both the ligand molecules and also comparable with the enzyme-acarbose complex (Fig.3a).

To assess the conformational stability and dynamic behavior of the enzyme-ligand complexes, root mean square fluctuation analysis was performed. This allows us to understand the positional fluctuations of Cα-atoms within the protein structure throughout the simulation. The RMSF plots for the three complexes: enzyme–acarbose, enzyme-compound 1, and enzyme-compound 2 are illustrated in Fig. 3b. The RMSF graph for the three complexes shows a similar trend to that of the enzyme–acarbose complex. The compounds showed stable binding characteristics, with minimal fluctuations for the amino acid residues at the binding site. The peaks observed for the residues 200–215, 370–380, and 830–840, align with the fluctuations seen in the enzyme–acarbose complex. These elevated values can be associated with the inherent flexibility of loop regions or terminal segments of the protein. The binding site residues of the enzyme show minimal deviation from their average positions during the binding of the two compounds.

The hydrogen bond interactions for all three enzyme–ligand complexes were analyzed, and the donor–acceptor bond distances were measured. The corresponding graphs illustrating these interactions are presented in Fig.3c. Acarbose forms a higher number of hydrogen bonds, especially after 70 ns, indicating strong and consistent interactions with the active site amino acids of the enzyme. Compound1 shows hydrogen bond interactions generally maintaining two to four hydrogen bonds throughout the trajectory. A maximum of five hydrogen bonds are seen to be formed between the enzyme and compound 1, and the stability in hydrogen bonding patterns implies that compound 1 maintains consistent interaction with the enzyme's active site. Compound 2 also shows consistent interactions with the enzyme by forming a maximum of six hydrogen bonds. Both compounds are found to maintain hydrogen bonds consistently throughout the simulation.

Fig. 3d represents the calculated radius of gyration for the enzyme-acarbose, enzyme-compound 1, and enzyme-compound 2 complexes. The Rg for the enzyme shows a similar trend for the three complexes, and it helped in understanding the compactness and structural stability for the complexes on ligand binding. The average Rg value over the past 50 ns for the enzyme-acarbose, -compound 1, and -compound 2 was found to be 2.88 nm, 2.86 nm, and 2.87 nm, respectively. Both the enzyme-compound complexes show a comparatively similar trend when compared to the enzyme-acarbose complex. The SASA graph for the three complexes is as shown in Fig. 3e. The SASA graph calculated measures the surface area accessible to the solvent molecules, thereby understanding the conformational changes and the structural integrity of the enzyme. All three complexes (enzyme-acarbose, -compound 1,

Table 6: Binding energies for the re-docked compounds identified from the ethyl acetate and ethanol extracts of *Swietenia macrophylla*

Compound name (Ethyl acetate extract)	Binding energy (kcal/mol)	Compound name (Ethanol extract)	Binding energy (kcal/mol)
3-phenyl-*N*-(1,3-thiazol-2-yl) propanamide	−5.43	1,5-Anhydro-4,6-O-benzylidene-D-glucitol	−5.64
4-Carbamoyl-2-phenyl-2-oxazoline	−5.67	9-Cycloheptatrienylidene-9,10-dihydro-10-oxoanthracene	−6.42
(6*S*)-3-methyl-6-[(2*S*)-6-methyl-4-oxohept-5-en-2-yl] cyclohex-2-en-1-one	−6.11	Phenyl-(5-phenylthiazol-2-yl)-amine	−5.80

Table 7: Hydrophobic and hydrogen bond interactions for the lead compounds considered for MD simulations

Compound name	Hydrophobic interactions	Hydrogen bonds
Cholest-5-ene-3,16,22,26-tetrol (Compound 1)	Tyr299, Trp406, Met444, Lys480, Phe575, and Tyr605	Asp203, Phe450, Arg526, Asp542, and Gln603
1,5-Anhydro-4,6-O-benzylidene-D-glucitol (Compound 2)	Tyr299, Asp327, Ile328, Ile364, Trp406, Asp443, Met444, Phe450, Arg526, and Phe575	Asp203 and Asp542
Acarbose	Ile328, Ile364, Trp406, Trp441, Asp443, Met444, Phe450, Arg526, Trp539, Phe575, and Gln603	Asp203, Tyr299, Asp327, Arg334, and Asp542

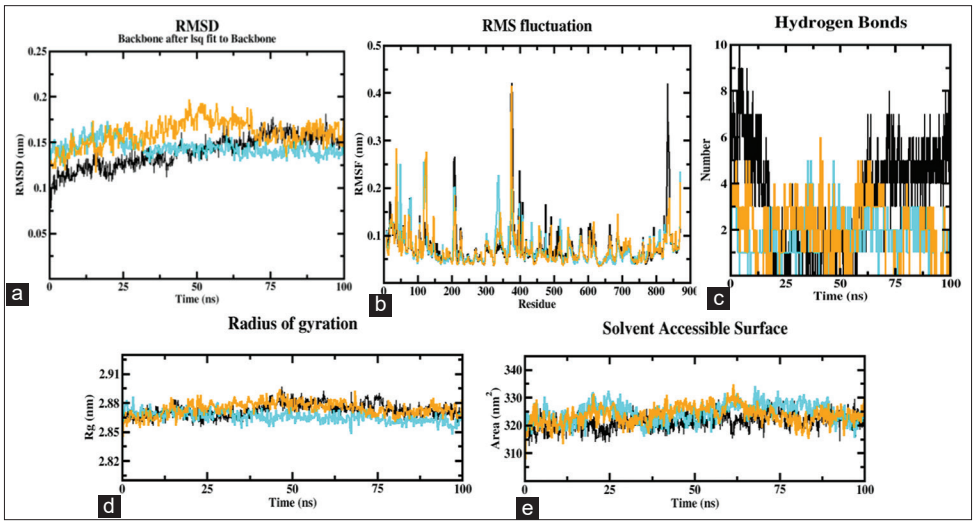

Fig. 3: (a) Root-mean-square deviation graph for the protein backbone atoms (b) Root-mean-square fluctuation for the Cα atoms (c) Hydrogen bond interactions formed between the enzyme and ligand compounds (d) Radius of gyration plot and (e) solvent-accessible surface area plot for the enzyme-compound 1 (cyan), -compound 2 (orange), and -acarbose (black) during the 100 ns simulation

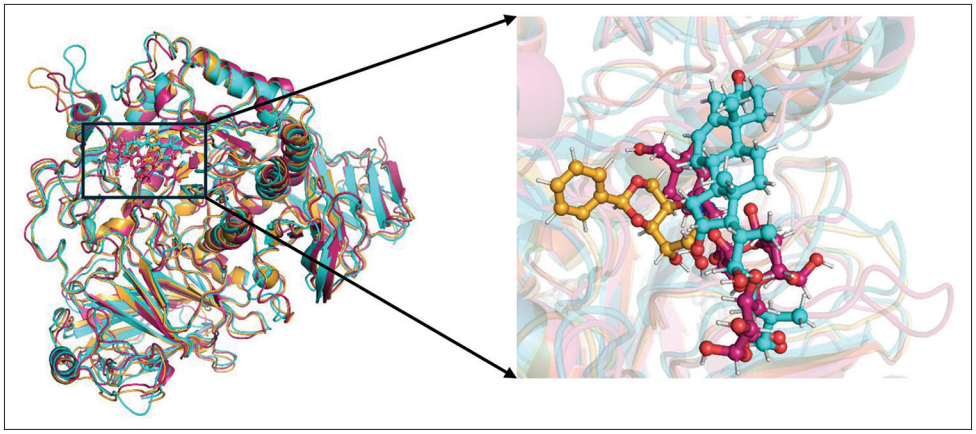

Fig. 4: Superposition of the best representative structures for the enzyme-acarbose (pink), enzyme-compound 1 (cyan), and enzyme-compound 2 (orange) complexes

and -compound 2) were found to have a stable SASA graph without much sharp fluctuations. The average SASA value for the three complexes for the past 50 ns was found to be 322.59 nm^2, 325.62 nm^2, and 324.25 nm^2, respectively.

The best representative structure for all the complexes was generated using cluster analysis in GROMACS. The final 50 ns of the trajectory was used for the analysis, and their superposition was performed using PyMOL [31] as shown in Fig. 4.

The RMSD values obtained after superimposing the best representative structures for enzyme-compound 1 (cyan) and enzyme-compound 2 (orange) complexes with enzyme-acarbose (pink) were 1.453 and 1.176 Å.

CONCLUSION

The fruits of *W. coagulans* and the seeds of *S. macrophylla* were subjected to sequential extraction to isolate bioactive compounds based on solvent polarity. Ethyl acetate and ethanol extracts from both plants were analyzed using GC-MS, and the identified compounds were screened *in silico* against the α-glucosidase enzyme using AutoDock Vina. The top three ligands from each extract, based on binding affinity and structure, were further validated through re-docking using AutoDock 4.2. Among the re-docked compounds, Cholest-5-ene-3,16,22,26-tetrol (compound 1) from *W. coagulans* and 1,5-Anhydro-4,6-O-benzylidene-D-glucitol (compound 2) from *S. macrophylla* showed binding energies of −6.66 and −5.64 kcal/mol, respectively. It was compared with that of the reference inhibitor acarbose (−4.27 kcal/mol). Based on their binding energy and favorable binding interactions with the active site residues, these two compounds were selected for further MD simulation studies.

The average RMSD values over the last 50 ns of the simulation indicated greater structural stability for the enzyme–compound 1 complex, while the enzyme–compound 2 complex displayed comparable stability to the reference. The high fluctuations observed in the RMSF plots were primarily localized to the loop regions/terminal ends of the protein. Radius of gyration (Rg) and solvent-accessible surface area (SASA) plots remained consistent over time, without significant deviations, suggesting sustained compactness and surface exposure of the complexes. Furthermore, the hydrogen bond interactions were maintained throughout the 100 ns simulation period, supporting the conformational stability of the enzyme–compound complexes. The superposition of the two complexes with the enzyme–acarbose complex shows that the ligand occupies the same binding site. These findings indicate that the selected compounds possess strong binding potential and structural compatibility with α-glucosidase and may serve as promising candidates for the development of potential antidiabetic therapeutics.

ACKNOWLEDGMENTS

The authors would like to thank DST-FIST, Government of India, for the computational facilities sanctioned to the department.

AUTHOR'S CONTRIBUTIONS

Roslin Elsa Varughese: Methodology, Experiment, Writing - Original draft, Reviewing and Editing. Gayathri Dasararaju: Supervision, Conceptualization, Methodology, Validation. Writing - Original draft, Reviewing and Editing.

CONFLICT OF INTEREST

Authors declare no conflict of interests.

AUTHOR'S FUNDING

The authors received no specific funding for this work.

REFERENCES

1. Akmal M, Patel P, Wadhwa R. Alpha glucosidase inhibitors. In: StatPearls. Treasure Island, FL: StatPearls Publishing; 2025. PMID 32496728
2. Maurya R, Akanksha, Jayendra, Singh AB, Srivastava AK. Coagulanolide, a withanolide from Withania coagulans fruits and antihyperglycemic activity. Bioorg Med Chem Lett. 2008 Dec 15;18(24):6534-7. doi: 10.1016/j.bmcl.2008.10.050, PMID 18952419
3. Hemalatha S, Wahi AK, Singh PN, Chansouria JP. Hypoglycemic activity of *Withania coagulans* Dunal in streptozotocin induced diabetic rats. J Ethnopharmacol. 2004 Aug;93(2-3):261-4. doi: 10.1016/j.jep.2004.03.043, PMID 15234762
4. Budhiraja RD, Sudhir S, Garg KN. Anti-inflammatory activity of 3 beta-hydroxy-2,3-dihydro-withanolide F. Planta Med. 1984 Apr;50(2):134-6. doi: 10.1055/s-2007-969651, PMID 6548033
5. Qureshi SA, Jahan M, Lateef T, Ahmed D, Rais S, Azmi MB. Presence of gallic acid and rutin improve the hepatoprotective strength of *Withania coagulans*. Pak J Pharm Sci. 2019 Jan;32(1Suppl):301-8. PMID 30829207
6. Aljohny BO, Anwar Y, Khan SA. *In vitro* anticancer and antibacterial potentials of selected medicinal plants and isolation and characterization of a natural compound from *Withania coagulans*. Z Naturforsch C J Biosci. 2022 Jan 14;77(7-8):263-70. doi: 10.1515/znc-2021-0259, PMID 34902232
7. Noreen H, Zaman B. Rahman AU, Hassan W. Antioxidant and antimicrobial efficacies of *Withania coagulans* seed extract against pathogenic bacteria and fungi. Int J Biotechnol Conscientia Beam. 2016 Oct 20;5(3):45-51. doi: 10.18488/journal.57/2016.5.3/57.3.45.51
8. Shohat B, Kirson I, Lavie D. Immunosuppressive activity of two plant steroidal lactones withaferin A and withanolide E. Biomedicine. 1978 Jan-Feb;28(1):18-24. PMID 27256
9. Pulivarthi V, Josthna P, Naidu CV. *In vitro* antidiabetic activity by glucose uptake of yeast cell assay and antioxidant potential

of *Annona reticulata* L. Leaf extracts. Int J Pharm Sci Drug Res. 2020 May;12(3):208-13. doi: 10.25004/IJPSDR.2020.120301
10. Heyninck K, Lahtela-Kakkonen M, Van Der Veken P, Haegeman G, Vanden Berghe W. Withaferin A inhibits NF-kappaB activation by targeting cysteine 179 in IKKβ. Biochem Pharmacol. 2014 Oct 15;91(4):501-9. doi: 10.1016/j.bcp.2014.08.004, PMID 25159986
11. White PT, Subramanian C, Motiwala HF, Cohen MS. Natural withanolides in the treatment of chronic diseases. Adv Exp Med Biol. 2016;928:329-73. doi: 10.1007/978-3-319-41334-1_14, PMID 27671823
12. Borah A, Selvaraj S, Holla SR, De S. Analysis of the bioactive components in *Swietenia macrophylla* leaves for their antibacterial and antioxidant capabilities. Bioresour Technol Rep. 2023 Jun;22:101411. doi: 10.1016/j.biteb.2023.101411
13. Maiti A, Dewanjee S, Jana GK, Mandal S. Hypoglycemic effect of *Swietenia macrophylla* seeds against type II diabetes. Int J Green Pharm. 2008;2(4):224. doi: 10.4103/0973-8258.44738
14. Moghadamtousi SZ, Goh BH, Chan CK, Shabab T, Kadir HA. Biological activities and phytochemicals of *Swietenia macrophylla* king. Molecules. 2013 Aug 30;18(9):10465-83. doi: 10.3390/molecules180910465, PMID 23999722
15. Pamplona S, Sá P, Lopes D, Costa E, Yamada E, E Silva C, *et al*. *In vitro* cytoprotective effects and antioxidant capacity of phenolic compounds from the leaves of *Swietenia macrophylla*. Molecules. 2015 Oct 16;20(10):18777-88. doi: 10.3390/molecules201018777, PMID 26501245
16. Sim L, Quezada-Calvillo R, Sterchi EE, Nichols BL, Rose DR. Human intestinal maltase-glucoamylase: Crystal structure of the N-terminal catalytic subunit and basis of inhibition and substrate specificity. J Mol Biol. 2008 Jan 18;375(3):782-92. doi: 10.1016/j.jmb.2007.10.069, PMID 18036614
17. Berman HM, Westbrook J, Feng Z, Gilliland G, Bhat TN, Weissig H, *et al*. The Protein Data Bank. Nucleic Acids Res. 2000 Jan 1;28(1):235-42. doi: 10.1093/nar/28.1.235, PMID 10592235
18. Kim S, Chen J, Cheng T, Gindulyte A, He J, He S, *et al*. PubChem 2023 update. Nucleic Acids Res. 2023 Jan 6;51(D1):D1373-80. doi: 10.1093/nar/gkac956, PMID 36305812
19. Pro CD. Version 8.0. Cambridge, MA: Cambridge Soft Corporation; 2004.
20. O'Boyle NM, Banck M, James CA, Morley C, Vandermeersch T, Hutchison GR. Open babel: An open chemical toolbox. J Cheminform. 2011 Oct 7;3:33. doi: 10.1186/1758-2946-3-33, PMID 21982300
21. Trott O, Olson AJ. AutoDock Vina: Improving the speed and accuracy of docking with a new scoring function, efficient optimization, and multithreading. J Comput Chem. 2010 Jan 30;31(2):455-61. doi: 10.1002/jcc.21334, PMID 19499576
22. Morris GM, Huey R, Lindstrom W, Sanner MF, Belew RK, Goodsell DS, *et al*. AutoDock4 and AutoDockTools4: Automated docking with selective receptor flexibility. J Comput Chem. 2009 Dec;30(16):2785-91. doi: 10.1002/jcc.21256, PMID 19399780
23. Laskowski RA, Swindells MB. LigPlot+: Multiple ligand-protein interaction diagrams for drug discovery. J Chem Inf Model. 2011 Oct 24;51(10):2778-86. doi: 10.1021/ci200227u, PMID 21919503
24. Abraham MJ, Murtola T, Schulz R, Páll S, Smith JC, Hess B, *et al*. GROMACS: high performance molecular simulations through multi-level parallelism from laptops to supercomputers. SoftwareX. 2015 Sep;1-2:19-25. doi: 10.1016/j.softx.2015.06.001
25. Bjelkmar P, Larsson P, Cuendet MA, Hess B, Lindahl E. Implementation of the CHARMM force field in GROMACS: Analysis of protein stability effects from correction maps, virtual interaction sites, and water models. J Chem Theor Comput. 2010 Feb 9;6(2):459-66. doi: 10.1021/ct900549r, PMID 26617301
26. Bugnon M, Goullieux M, Röhrig UF, Perez MA, Daina A, Michielin O, *et al*. SwissParam 2023: A modern web-based tool for efficient small molecule parametrization. J Chem Inf Model. 2023 Nov 13;63(21):6469-75. doi: 10.1021/acs.jcim.3c01053, PMID 37853543
27. Zoete V, Cuendet MA, Grosdidier A, Michielin O. SwissParam: A fast force field generation tool for small organic molecules. J Comput Chem. 2011 Aug;32(11):2359-68. doi: 10.1002/jcc.21816, PMID 21541964
28. Xmgrace TP. Version 5.1.19. Center for Coastal and Land-Margin Research. Beaverton, OR: Oregon Graduate Institute of Science and Technology; 2005.
29. Susilawati Y, Megantara S, Levita J. Antidiabetic activity of novel chromene compound isolated from *Peperomia pellucida l*. Kunth and *in silico* study against dpp-iv, alpha-glucosidase, alpha-amylase, and aldose reductase for blood glucose homeostasis. Int J Appl Pharm. 2022;14(5):110-6. doi: 10.22159/ijap.2022.v14s5.22
30. Mukka D, Devarakonda KP. GC-MS analysis and molecular docking studies of *Laserpitium latifolium L*. Extract for anti-diabetic activity. Int J Appl Pharm. 2025;17(1):190-8. doi: 10.22159/ijap.2025v17i1.52343
31. The PyMOL Molecular Graphics System. Version 3.0. Schrödinger, LLC; 2021.